Chinese Chemical Letters 34 (2023) 107777

Contents lists available at ScienceDirect

Chinese Chemical Letters

journal homepage: www.elsevier.com/locate/cclet

Dual-template synthesis of defect-rich mesoporous Co_3O_4 for low temperature CO oxidation

Shuhua Song[a], Jian Liang[a], Wei Xiao[b], Dong Gu[a,*]

[a] The Institute for Advanced Studies, Wuhan University, Wuhan 430072, China
[b] College of Chemistry and Molecular Sciences, Wuhan University, Wuhan 430072, China

ARTICLE INFO

Article history:
Received 18 July 2022
Revised 27 July 2022
Accepted 22 August 2022
Available online 24 August 2022

Keywords:
Mesoporous
Dual-template
Co_3O_4
CO oxidation
Defect

ABSTRACT

CO oxidation is a benchmark in heterogeneous catalysis for evaluation of redox catalysts due to its practical relevance in many applications and the fundamental problems associated with its very high activity at low temperatures. Among which, Co_3O_4 is one of the most active non-precious metal catalysts. Exposed crystal planes and cobalt sites are considered to be important for its high catalytic activity. Herein, we demonstrate an enhanced CO oxidation activity by a defect-rich mesoporous Co_3O_4 that prepared by a designed dual-template method. Two different kinds of silicas are used as hard-templates at the same time, resulting in a defect-rich mesoporous Co_3O_4 with a surface area as high as 169 m^2/g. This catalyst exhibited a very high catalytic activity for low temperature CO oxidation with a light-off temperature at −73 °C under the space velocity of 80,000 mL h^{-1} g_{cat}^{-1}. Further studies reveal that the high surface area promotes the lattice oxygen mobility, surface rich of Co^{2+} species and active oxygen species are crucial for the high catalytic activity. Moreover, the dual-template approach paves a way towards the design and construction of high-surface-area mesoporous metal oxides for various applications.

CO oxidation to CO_2 has been broadly investigated for decades due to its great value not only in fundamental catalytic research as a probe reaction, but also in practical applications, such as air purification, automotive exhaust emissions control and preferential oxidation in proton-exchange-membrane fuel cells [1–5]. Among these applications, especially in controlling automobile exhaust, large amounts of CO are generally produced during the cold starting, which lead to serious environmental problems. In order to regulate CO emission, developing high performance catalysts that can convert CO into CO_2 at low temperature is significant. Although supported noble metal catalysts show superior performance for CO oxidation and have been thoroughly investigated [6–10], their applications have been restrained by high cost and limited sources. As alternative, catalyst systems, with decent catalytic performance and high availability but low cost, have been extensively studied.

Among these catalyst systems, transition metal oxides are mostly studied for CO oxidation [11–15]. Co_3O_4 with spinel structure has been considered to be the most promising alternative to noble metals due to its high catalytic activity at relatively low temperature, which comes from its suitable strength of adsorbing CO, low barrier to activate oxygen and superior redox capacity [16]. Considerable work has been done towards CO oxidation over cobalt-based materials [17–24]. Thormählen *et al.* prepared a pre-oxidized Al_2O_3-supported Co_3O_4 catalysts, which showed a light-off temperature (T_{50}) of −63 °C [25]. Xie *et al.* reported a Co_3O_4 nanorods with exposed (100) planes rich in Co^{3+} could completely catalyze CO oxidation at −77 °C [26]. Jia *et al.* synthesized Co_3O_4/SiO_2 nanocomposite with enriching silica and Co^{2+} species on surface, which exhibited a high activity for total conversion of CO at −76 °C [27]. Ordered mesoporous CoO with octahedrally coordinated Co^{2+} species displayed unexpectedly high activity for CO oxidation due to its easy oxidation of surface Co^{2+} to Co^{3+}, suggesting the importance of coordination environment of the active sites [28]. Considering the reactant diffusion process is a crucial factor affecting the catalytic performance, a porous structure is expected to increase the amount of accessible active sites and benefit the reactant-catalyst contact, thus enhancing catalytic activity. For example, Ren *et al.* used a series of mesoporous metal oxides (*i.e.*, Co_3O_4, CuO) as catalysts for CO oxidation, which exhibited higher activities than their bulk counterparts [29]. Template methods have been widely used in materials synthesis [30–35]. Hard-templating method (nanocasting), by using ordered mesoporous solids as nanoreactors, can create nanosized porous metal oxides with high surface areas and long-range ordering [36–40]. Additionally, the prepared mesoporous metal oxides own similar texture and structure with their templates. However, the specific

* Corresponding author.
E-mail address: DGu@whu.edu.cn (D. Gu).

https://doi.org/10.1016/j.cclet.2022.107777
1001-8417/

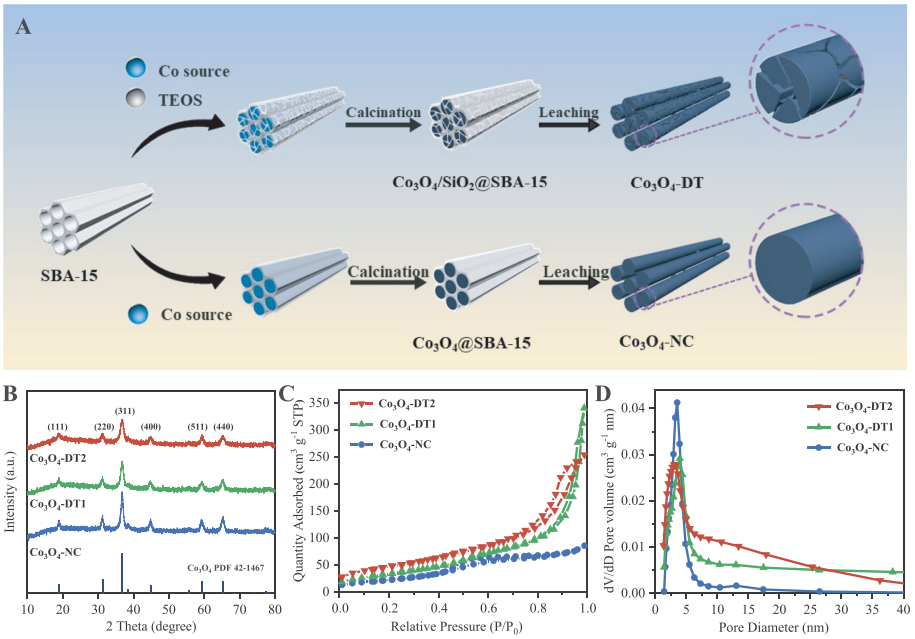

Fig. 1. (A) Schematic illustration of synthetic process for mesoporous Co_3O_4 by dual-template method (Co_3O_4-DT) and the traditional nanocasting method (Co_3O_4-NC). (B) XRD patterns of Co_3O_4-NC, Co_3O_4-DT1 and Co_3O_4-DT2. (C) Nitrogen adsorption-desorption isotherms and (D) corresponding pore size distributions curves of Co_3O_4-NC, Co_3O_4-DT1 and Co_3O_4-DT2.

surface area of nanocast metal oxides is confined, since primary particles metal oxides are prone to sinter during thermal treatment. For the sake of attaining mesoporous metal oxides with high specific surface area providing abundant reactive sites to enhance their catalytic performance, traditional nanocasting method needs improvement.

Herein, we report a dual-template method to synthesize mesoporous Co_3O_4 (Co_3O_4-DT), which is rich in defects and possesses very high specific surface area. A modification to the traditional nanocasting method was used to create defects inside the nanorods of the nanocast mesoporous Co_3O_4. Both mesoporous silica SBA-15 and *in situ* generated SiO_2 are used as hard templates at the same time. After the removal of templates by NaOH, a secondary pore was generated, which created more exposed surface. The specific surface area of the obtained Co_3O_4 is as high as 169 m^2/g, which is more than two times higher than that of Co_3O_4-NC that synthesized by normal nanocasting method. The Co_3O_4-DT catalyst exhibits prominent catalytic activity for CO oxidation, superior to Co_3O_4-NC. Further investigations reveal the factors that affecting the performance of CO oxidation. What is more, the dual-template method can be extended to synthesize other mesoporous metals oxides including iron, nickel and cerium oxides, *etc*., providing scientific insights into rational design of meso–structures with high specific surface area for superior catalytic activity.

The synthesis schematic of Co_3O_4-DT and Co_3O_4-NC is shown in Fig. 1A and detailed process is elaborated in the Supporting information. According to the different amounts of tetraethoxysilane (TEOS), the obtained Co_3O_4-DT by dual-template were denoted as Co_3O_4-DT1 (low amount of TEOS) and Co_3O_4-DT2 (high amount of TEOS), respectively. XRD patterns of all replica materials (Fig. 1B) show well-resolved reflection peaks, which can be assigned to spinel Co_3O_4 phase (PDF#42-1467) with a Fd3m symmetry. No other diffraction peaks were detected, indicating high purity phase. With increasing TEOS amount, the diffraction peaks of the replica Co_3O_4 obviously become weaker and broader, revealing a lower level of crystallization and/or smaller crystalline grain size. The grain sizes were calculated based on the (311) facets of Co_3O_4 by using Scherrer equation, as listed in Table 1. It is shown that the grain sizes of Co_3O_4-DT2 (8.9 nm) are smaller than that of Co_3O_4-DT1 (10.9 nm) and Co_3O_4-NC (12.7 nm), indicating that the introduction of TEOS can effectively suppress Co_3O_4 nanocrystals sintering during the calcination process. And this phenomenon on cobalt catalysts also have been observed in literature [41,42]. The N_2 adsorption-desorption isotherms and corresponding pore size distributions curves of the replica samples are showed in Figs. 1C and D. And the relevant parameters are summarized in Table 1. For Co_3O_4-NC, the specific surface area and pore volume are calculated to be 81 m^2/g and 0.13 cm^3/g, respectively. Interestingly, the specific surface area of Co_3O_4-DT1 and Co_3O_4-DT2 prepared by dual-template method are significantly increased to 122 and 169 m^2/g, and the corresponding pore volumes are also increased remarkably to 0.52 and 0.39 cm^3/g, respectively. The pore sizes distribution of this catalyst has a maximum around 3–4 nm, revealing a uniform mesoporous structure. The morphological and structural features were further analyzed by transmission electron microscopy (TEM). It can be seen that Co_3O_4-NC presents a rod-like morphology (Figs. 2A and B), and the rod diameter is consistent with the pore size of SBA-15, suggesting a good replication of the SBA-15 template. In addition, all the nanorods are quite dense without obvious cracks or grain boundaries. Lattice fringes show a *d*-spacing of 0.24 nm in high-resolution TEM (HR-TEM) image (Fig. 2C), which is in well accordance with the (311) crystal planes of spinel Co_3O_4 [43,44]. Co_3O_4-DT1 prepared by dual-template method also exhibits a rod-like morphology (Figs. 2D and E). However, compared to traditional Co_3O_4-NC, plenty of randomly oriented cracks/pores are observed in the nanorod arrays of Co_3O_4-DT1, and these cracks/pores can connect the meso–channels to build an interconnected mesopore networks. When further increase the amount of TEOS, the cracks/pores inside the nanorods are increases remarkably (Figs. 2G and H). The crystals lattice fringes for both Co_3O_4-DT1 and Co_3O_4-DT2 catalysts can be clearly observed in the HR-TEM images (Figs. 2F and I). An average D-spacing is measured to be 0.29 nm, which can be assigned to the (220) reflection of Co_3O_4 spinel structure [45,46]. The existence of the inner nanorods pores are contributed to the increase of the specific surface area. These

Table 1
Physicochemical properties and CO oxidation activities of different Co_3O_4 catalysts.

Sample name	Surface area (m^2/g)	Pore volume (cm^3/g)	Crystal size[a] (nm)	Co^{2+}/Co^{3+} molar ratio	O_{ads}/O_{lat} molar ratio	T_{50} (°C)	E_a (kJ/mol)
Co_3O_4-NC	81	0.13	12.7	0.38	0.59	−50	50.3
Co_3O_4-DT1	122	0.52	10.9	0.43	0.73	−65	41.6
Co_3O_4-DT2	169	0.39	8.9	0.55	1.10	−73	33.9
Commercial Co_3O_4	3	0.01	>30	–	–	212	–
Fe_2O_3-DT	368	1.00	–	–	–	–	–
NiO-DT	208	0.58	–	–	–	–	–
CeO_2-DT	291	0.66	–	–	–	–	–

[a] The grain size was calculated by the FMWH of Co_3O_4 (311) peak using the Scherrer equation.

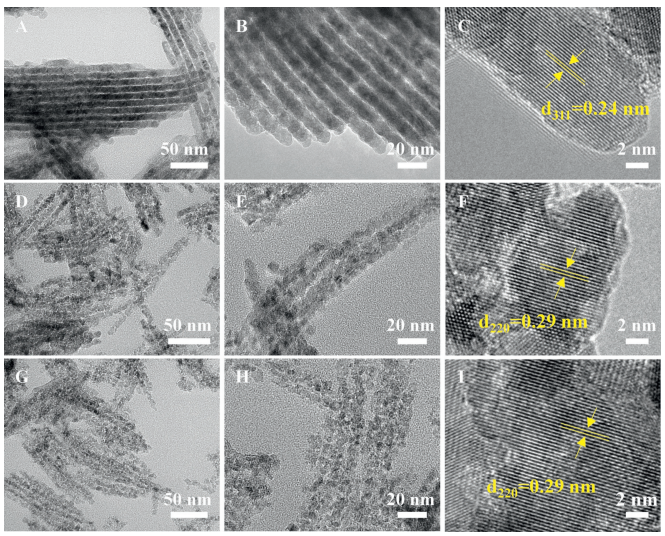

Fig. 2. TEM and HR-TEM images of (A-C) Co_3O_4-NC, (D-F) Co_3O_4-DT1 and (G-I) Co_3O_4-DT2.

results reveal that the introduction of TEOS during synthesis process gives rise to numerous cracks, whose density can be controllably adjusted while maintaining structural integrity. The more open porous structures leading by cracks are expected to favor the facile accessibility of active sites. These results indicate the successful synthesis of Co_3O_4-DT with high specific surface area and high porosity by dual-template method. Moreover, this strategy can be extended to the synthesis of other mesoporous metal oxides with high specific surface area. Mesoporous Fe_2O_3 (Fe_2O_3-DT), NiO (NiO-DT), and CeO_2 (CeO_2-DT) with similar structure and enhanced specific surface areas can also be synthesized. The related structure characterizations are showed in Fig. S1 (Supporting information) and Table 1.

The large specific surface area and high porosity of Co_3O_4-DT can provide abundant active sites, making them promising candidates for catalysis. CO oxidation catalytic performances of these samples were evaluated under both normal and dry feed gas conditions. Meanwhile, the catalytic performances of Co_3O_4-NC and commercial Co_3O_4 were also explored for comparison. The catalytic activities of the catalysts for CO oxidation were measured in a plug flow reactor using a gas mixture of 1 vol% CO, 20 vol% O_2 and 79 vol% He. The results are shown in Fig. 3 and summarized in Table 1. Among these catalysts, Co_3O_4-DT2 shows the optimum catalytic activity with a T_{50} value of as low as −73 °C at a high space velocity of 80 000 mL h^{-1} g_{cat}^{-1}, and a full CO conversion at −43 °C. The T_{50} value of Co_3O_4-DT1 slightly increases to −65 °C. Co_3O_4-NC prepared by conventional nanocasting method could only reach 50% CO conversion at −50 °C. In addition, all these mesoporous materials show much higher catalytic activities than that of the commercial Co_3O_4, which is only unable to fully convert CO to CO_2 until the temperature reaches 225 °C. Apparently, the T_{50} of CO conversion markedly decreases with increasing specific surface area of catalysts, indicating that catalytic activity can be improved by higher specific surface area promoting the exposure of abundant reactive sites. The excellent stability of the dual-template Co_3O_4 catalysts is generally required in practical applications, so long-term durability performances were further investigated. The obtained results are showed in Fig. 3B. Co_3O_4-DT2 catalyst maintains full CO conversion for up to 32 consecutive hours at 30 °C under dry feed gas condition. When the test was performed under normal feed gas condition with about 3 ppm water, complete CO conversion remains during the initial 24 h, much longer than that reported in literature [43]. After that, the CO conversion suddenly drops to 85% and then slightly to 72% after 32 h. Such a deactivation can be explained by the poisoning effects of H_2O/OH^- species or carbonate intermediates on the catalyst surface, which block the catalytic active sites [47–49]. With the aim to provide deeper insights into CO oxidation catalytic properties of the as-prepared catalysts, the kinetic experiments were conducted to determine the apparent activation energy (E_a) for CO oxidation (Fig. 3C), which are calculated from the Arrhenius plots and listed in Table 1. Co_3O_4-DT2 displays enhanced reaction kinetic with the lowest apparent activation energy (33.9 kJ/mol), followed by Co_3O_4-DT1 (41.6 kJ/mol) and Co_3O_4-NC (50.3 kJ/mol). The lowest apparent activation energy of Co_3O_4-DT2 is in good according with the light-off results.

The above results show that high-surface-area mesoporous Co_3O_4 catalysts prepared by dual-template can effectively improve the catalytic activity for low temperature CO oxidation. Since the catalytic activity is affected by many factors such as metal valent states and absorbed species states, therefore, further investigation of the origin of the high catalytic performance is needed. The chemical state and surface properties of the catalysts were investigated by X-ray photoelectron spectroscopy (XPS). The oxidation states of cobalt were evaluated by Co 2p spectra which were split into Co^{2+} and Co^{3+} peaks, as shown in Fig. 4A. The Co $2p_{3/2,1/2}$ peaks with binding energies at 780.1 and 795.5 eV can be assigned to Co^{3+} species, while the peaks at 781.8 and 797.2 eV are ascribed to Co^{2+}species [43]. The surface Co^{2+}/Co^{3+} molar ratios of samples are calculated based on the fitting of Co 2p spectra and listed in Table 1. As one can see, when the specific surface areas increase, surface Co^{2+}/Co^{3+} molar ratios are increased in the order of Co_3O_4-NC (0.38) < Co_3O_4-DT1 (0.43) < Co_3O_4-DT2 (0.55), implying the relative enrichment of Co^{2+} species on Co_3O_4-DT2. For the O 1s spectra in Fig. 4B, it can be mainly deconvoluted into two peaks standing for the existence of different surface oxygen species. The peaks with banding energy at ~529.7 and 531.2 eV are attributed to surface lattice oxygen (O_{lat}) and adsorbed oxygen (O_{ads}, *e.g.*, O^-, O_2^-), respectively [50]. The O_{ads} species with higher binding energy are generally supposed to be more active than O_{lat} and may play a key role in determining the low-temperature performance of CO oxidation [49,51,52]. The O_{ads}/O_{lat} molar ratios of these catalysts are calculated according to quanti-

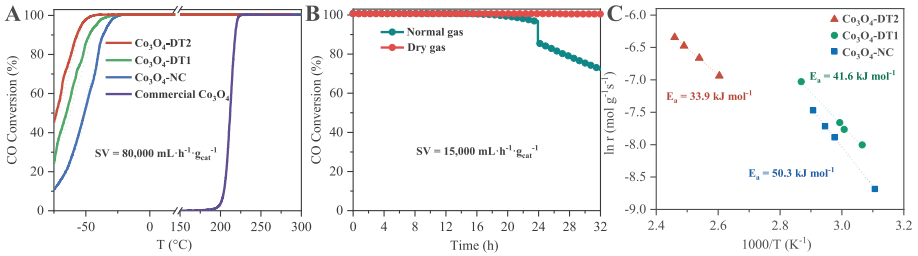

Fig. 3. (A) Temperature dependence of the activity for CO oxidation under both normal (dotted line) and dry (solid line) conditions for Co_3O_4-NC, Co_3O_4-DT1, Co_3O_4-DT2, and commercial Co_3O_4. (B) The long-term stability test of Co_3O_4-DT2 at 30 °C under normal and dry conditions. (C) Arrhenius plots for the rate of CO oxidation over the catalysts: (■) Co_3O_4-NC, (●) Co_3O_4-DT1, (▲) Co_3O_4-DT2.

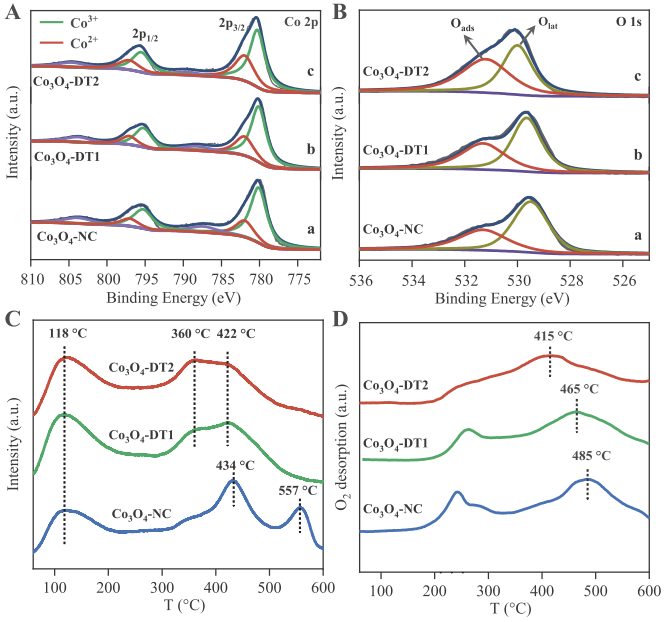

Fig. 4. (A) Co 2p, (B) O 1s spectra, (C) CO-TPD and (D) O_2-TPD measurements of Co_3O_4-NC, Co_3O_4-DT1 and Co_3O_4-DT2.

tative analysis of corresponding peaks areas, as shown in Table 1. The molar ratios of O_{ads}/O_{lat} follow the order of Co_3O_4-NC (0.59) < Co_3O_4-DT1 (0.73) < Co_3O_4-DT2 (1.10), which is identical to that of Co^{2+}/Co^{3+} molar ratio. This order is reasonable in light of the overall surface charge neutrality. Assuming adsorbed oxygen species are produced by oxygen vacancies, it is suggested that the number density of oxygen vacancies on Co_3O_4-DT2 is higher than that of others. The spectra of Co 2p and O 1s suggest that both higher Co^{2+}/Co^{3+}molar ratio and abundant oxygen vacancies are important in enhancing the catalytic activity of Co_3O_4 catalyst.

The CO-TPD experiments were conducted to investigate the surface oxygen activity of catalysts for CO oxidation. During the heating process, the majority of CO adsorbed on catalysts surface desorbed as CO_2, which were produced by the reaction of adsorbed CO with surface lattice oxygen [53]. As shown in Fig. 4C, the CO-TPD profile of Co_3O_4-NC shows three peaks located at 118, 434, and 557 °C, indicating three kinds of lattice oxygen with different environments. All catalysts display an identical CO_2 desorption peak at around 118 °C, and other two broad peaks for Co_3O_4-DT1 and Co_3O_4-DT2 are located at 360 and 422 °C. Compared with Co_3O_4-NC, the CO_2 desorbed temperatures of Co_3O_4-DT1 and Co_3O_4-DT2 shift to lower value, implying that adsorbed CO are more easily oxidized by surface lattice oxygen. Since oxygen mobility on the metal oxides plays a crucial role in oxygen-involving catalytic reactions [54–57], O_2-TPD experiments were performed to study the mobility of different oxygen species on catalysts. Generally, oxygen species adsorbed on surface can go through succeeding transformation with electron gain ability: $O_2(ad) \rightarrow O_2^-(ad) \rightarrow O^-(ad) \rightarrow O^{2-}(ad/lattice)$. $O_2(ad)$ is ascribed to the physically adsorbed oxygen, which can be removed by purging before test. The adsorbed species of $O_2^-(ad)$ and $O^-(ad)$ are poorly bonded on the catalysts surface, while $O^{2-}(ad)$ species are usually regarded as a kind of surface lattice oxygen, which are difficult to be removed. Based on the literature results [51,58], the peaks at temperature below 300 °C are related to the desorption of surface adsorbed $O_2^-(ad)$ and $O^-(ad)$ species, while the peaks above 350 °C are attributed to surface lattice oxygen and lattice oxygen in bulk phase (>700 °C). As shown in Fig. 4D, a clear moderating trend in desorption temperature of surface lattice oxygen species can be observed: Co_3O_4-DT2 (415 °C) < Co_3O_4-DT1 (465 °C) < Co_3O_4-NC (485 °C), indicating Co_3O_4-DT2 possesses the most active surface lattice oxygen. Increasing surface areas of samples can alleviate Co-O bond and thus promote the desorption of lattice oxygen from Co_3O_4 [59]. Hence, the increased mobility of surface lattice oxygen on Co_3O_4-DT2 can be relevant to surface area effect. Based on the CO-TPD and O_2-TPD results, higher specific surface area accelerates lattice oxygen mobility, leading to much easier CO oxidation.

It is well-known that the adsorption and activation of molecular oxygen are essential to Co-based catalysts for CO oxidation. The generation of adsorbed reaction oxygen species, such as superoxide ions (O_2^-), can be related to the presence of surface oxygen vacancies on metal oxides supports or at the interfaces between metal and the support. A wide variety of superoxide species have been reported to exist between −196 °C and 25 °C on the surface of CoO-MgO solid solutions [60], Co_3O_4/SiO_2 composite materials [27], and reduced Co_3O_4 (100) [61]. It is thus hypothesized that such superoxide species may play a crucial role in CO oxidation and also over the mesoporous Co_3O_4 studied here at low temperature. For this consideration, CO titration experiments in the absence of O_2 (1 vol% CO in N_2) were conducted to evaluate the availability of oxygen stored on the catalysts. The transient responses of CO_2 and CO evolution over these three pretreated Co_3O_4 catalysts at different temperatures are showed in Fig. S2 (Supporting information). For Co_3O_4-DT2, a maximum (CO_2 concentration 0.08%) of CO_2 evolution is observed at 108 s after exposure to CO at −50 °C, indicating a high capacity of reactive oxygen. The prompt CO_2 responses show a fast reaction proceeding *via* CO rapid adsorption, followed by the reaction of CO with reactive oxygen species on the catalyst surface. At 30 and 120 °C, strong CO_2 evolutions are noticed after 84 s with CO_2 concentration of 0.32% and 0.63%, respectively, higher than that observed at −50 °C. Similar trends of CO_2 respond at different temperature are also observed for Co_3O_4-NC and Co_3O_4-DT1. The capacity of these catalysts to provide reactive oxygen is enhanced as increasing temperature, consistent well with the temperature dependence of CO oxidation activity. Moreover, the maxima of CO_2 evolution

for Co_3O_4-DT2 at corresponding temperature are integrally higher than that of others, suggesting the strongest ability of Co_3O_4-DT2 to provide reactive oxygen. The integral under the curves showed in Fig. S2 allow to calculate the total amount of active oxygen on surface of catalysts. To assess whether bulk oxygen contributes to CO oxidation in the titration experiments, the maximum amount of oxygen only present on the surface was calculated assuming that the surface of catalyst only consists of closely-packed (111) planes of Co_3O_4. For all the catalysts at different temperatures, the total amounts of consumed oxygen are lower than the theoretical maximum amount (Table S1 in Supporting information). It can be attributed to the presence of other planes such as (100) or (110) with lower oxygen density. The calculated oxygen consumption in 1200 s shows higher values for Co_3O_4-DT2 than that for Co_3O_4-DT1 and Co_3O_4-NC at −50, 30 and 120 °C, suggesting Co_3O_4-DT2 contains more reactive oxygen. A high ability to supply reactive oxygen would be responsible for the extraordinary activity of CO oxidation at low temperatures, which explains the different activity of these catalysts in a plausible way.

To further investigate the reaction mechanism, *in situ* DRIFT experiments were performed on Co_3O_4-NC and Co_3O_4-DT2. The obtained DRIFT spectra were collected to get the direct information about the reaction intermediates and side products during the exposure to CO and O_2 with a ramping temperature (20–310 °C). The signals of two peaks at 2171 and 2110 cm^{-1} (Figs. S3A and C in Supporting information) attributed to CO characteristic bands are very weak due to the rapid CO conversion. And CO_2 characteristic peaks centered at around 2360 and 2337 cm^{-1} are obviously detected at the very beginning of reaction. Both catalysts show a set of bands in the range of 1300–1700 cm^{-1} (Figs. S3B and D in Supporting information). These bands have been assigned to various carbonate vibrations, which become stronger with increasing temperature, indicating the accumulation of carbonates on the catalysts surface. These carbonate species are kept stable on the catalysts surface even at 310 °C. In view of the oppositional results in literature, it is hard to precisely assign these bands. However, during the reaction process, Co_3O_4-NC and Co_3O_4-DT2 have definitely different carbonate vibrations, which may also affect the catalytic reaction process.

In summary, a dual-template method was developed for the successful synthesis of ordered mesoporous Co_3O_4 with enhanced defects and high specific surface area by using SBA-15 and *in situ* generate SiO_2 as hard templates. The obtained samples were proved to be significantly active for low-temperature CO oxidation, superior to that prepared by traditional nanocasting method. The enhanced catalytic performance is mainly associated with high specific surface area, abundant Co^{2+} species and active oxygen species. Both high specific surface area and abundant oxygen vacancies are conducive to accelerate the mobility of lattice oxygen. Such a controllable dual-template method can be extended to construct other mesoporous metal-oxides-based materials with high specific surface areas for various applications.

Declaration of competing interest

The authors declare that they have no known competing financial interests or personal relationships that could have appeared to influence the work reported in this paper.

Acknowledgments

The authors acknowledge funding from the National Key R&D Program of China (No. 2018YFE0201703), the "1000-Youth Talents Plan", and the Fundamental Research Funds for the Central Universities (No. 2042019kf0230).

Supplementary materials

Supplementary material associated with this article can be found, in the online version, at doi:10.1016/j.cclet.2022.107777.

References

[1] B.T. Qiao, A.Q. Wang, X.F. Yang, et al., Nat. Chem. 3 (2011) 634–641.
[2] K. An, S. Alayoglu, N. Musselwhite, et al., J. Am. Chem. Soc. 135 (2013) 16689–16696.
[3] C.L. Wang, X.K. Gu, H. Yan, et al., ACS Catal. 7 (2017) 887–891.
[4] L. Nie, D.H. Mei, H.F. Xiong, et al., Science 358 (2017) 1419–1423.
[5] G. Spezzati, A.D. Benavidez, A.T. DeLaRiva, et al., Appl. Catal. B: Environ. 243 (2019) 36–46.
[6] H.H. Kung, M.C. Kung, C.K. Costello, J. Catal. 216 (2003) 425–432.
[7] N. Lopez, T.V.W. Janssens, B.S. Clausen, et al., J. Catal. 223 (2004) 232–235.
[8] H.Y. Kim, H.M. Lee, G. Henkelman, J. Am. Chem. Soc. 134 (2012) 1560–1570.
[9] D. Gu, J.C. Tseng, C. Weidenthaler, et al., J. Am. Chem. Soc. 138 (2016) 9572–9580.
[10] Y.S. Zhang, J.X. Liu, K. Qian, et al., Angew. Chem. Int. Ed. 60 (2021) 12074–12081.
[11] J.W. Saalfrank, W.F. Maier, Angew. Chem. Int. Ed. 43 (2004) 2028–2031.
[12] D. Gu, C.J. Jia, H. Bongard, et al., Appl. Catal. B: Environ. 152-153 (2014) 11–18.
[13] Y. Lou, L. Wang, Z.Y. Zhao, et al., Appl. Catal. B: Environ. 146 (2014) 43–49.
[14] Y.F. Sun, T. Wu, Z.H. Bao, et al., ACS Cent. Sci. 8 (2022) 1081–1090.
[15] X.Y. Tang, J.C. Wang, Y.H. Ma, et al., Chin. Chem. Lett. 32 (2021) 48–52.
[16] H.F. Wang, R. Kavanagh, Y.L. Guo, et al., J. Catal. 296 (2012) 110–119.
[17] J. Jansson, J. Catal. 194 (2000) 55–60.
[18] J. Jansson, M. Skoglundh, E. Fridell, P. Thormählen, Top. Catal. 16 (2001) 385–389.
[19] J. Jansson, A.E.C. Palmqvist, E. Fridell, et al., J. Catal. 211 (2002) 387–397.
[20] H. Tüysüz, M. Comotti, F. Schüth, Chem. Commun. (2008) 4022–4024.
[21] L.H. Hu, K.Q. Sun, Q. Peng, et al., Nano Res. 3 (2010) 363–368.
[22] L. Lukashuk, N. Yigit, R. Rameshan, et al., ACS Catal. 8 (2018) 8630–8641.
[23] T. Baidya, T. Murayama, S. Nellaiappan, et al., J. Phys. Chem. C 123 (2019) 19557–19571.
[24] H. Kersell, Z. Hooshmand, G. Yan, et al., J. Am. Chem. Soc. 142 (2020) 8312–8322.
[25] P. Thormählen, M. Skoglundh, E. Fridell, B. Andersson, J. Catal. 188 (1999) 300–310.
[26] X. Xie, Y. Li, Z.Q. Liu, et al., Nature 458 (2009) 746–749.
[27] C.J. Jia, M. Schwickardi, C. Weidenthaler, et al., J. Am. Chem. Soc. 133 (2011) 11279–11288.
[28] D. Gu, C.J. Jia, C. Weidenthaler, et al., J. Am. Chem. Soc. 137 (2015) 11407–11418.
[29] Y. Ren, Z. Ma, L.P. Qian, et al., Catal. Lett. 131 (2009) 146–154.
[30] D. Gu, H. Bongard, Y. Meng, et al., Chem. Mater. 22 (2010) 4828–4833.
[31] Z.K. Sun, Y. Liu, B. Li, et al., ACS Nano 7 (2013) 8706–8714.
[32] W. Luo, Y.H. Li, J.P. Dong, et al., Angew. Chem. Int. Ed. 52 (2013) 10505–10510.
[33] J. Wei, Y. Ren, W. Luo, et al., Chem. Mater. 29 (2017) 2211–2217.
[34] Y.T. Zhang, Y. Wu, Y.Q. Su, et al., Small 18 (2022) 2105178.
[35] X. Zhang, W. Weng, H. Gu, et al., Adv. Mater. 34 (2022) 2104427.
[36] H.F. Yang, D.Y. Zhao, J. Mater. Chem. 15 (2005) 1217–1231.
[37] A.H. Lu, F. Schüth, Adv. Mater. 18 (2006) 1793–1805.
[38] D. Gu, F. Schüth, Chem. Soc. Rev. 43 (2014) 313–344.
[39] D. Gu, W. Schmidt, C.M. Pichler, et al., Angew. Chem. Int. Ed. 56 (2017) 11222–11225.
[40] Y.H. Peng, S.H. Song, F.Q. Liu, et al., Chem. Mater. 34 (2022) 7042–7057.
[41] H. Bu Xing, Acta Phys. Chim. Sin. 37 (2021) 2010063.
[42] L.X. Wang, E.J. Guan, Y.Q. Wang, et al., Nat. Commun. 11 (2020) 1033.
[43] W.Q. Song, A.S. Poyraz, Y.T. Meng, et al., Chem. Mater. 26 (2014) 4629–4639.
[44] M.J. Zhou, L.L. Cai, M. Bajdich, et al., ACS Catal. 5 (2015) 4485–4491.
[45] W.X. Tang, J.F. Weng, X.X. Lu, et al., Appl. Catal. B: Environ. 256 (2019) 117859.
[46] L.P. Zhong, T. Kropp, W. Baaziz, et al., ACS Catal. 9 (2019) 8325–8336.
[47] F. Grillo, M.M. Natile, A. Glisenti, Appl. Catal. B: Environ. 48 (2004) 267–274.
[48] H.F. Wang, R. Kavanagh, Y.L. Guo, et al., Angew. Chem. Int. Ed. 51 (2012) 6657–6661.
[49] Y.F. Cai, J. Xu, Y. Guo, J.Y. Liu, ACS Catal. 9 (2019) 2558–2567.
[50] J. Bae, D. Shin, H. Jeong, et al., ACS Catal. 9 (2019) 10093–10100.
[51] Y.Z. Wang, Y.X. Zhao, C.G. Gao, D.S. Liu, Catal. Lett. 125 (2008) 134–138.
[52] Y. Yu, T. Takei, H. Ohashi, et al., J. Catal. 267 (2009) 121–128.
[53] S.S. Sun, D.S. Mao, J. Yu, et al., Catal. Sci. Technol. 5 (2015) 3166–3181.
[54] H. Song, U.S. Ozkan, J. Catal. 261 (2009) 66–74.
[55] W.Z. Si, Y. Wang, S. Zhao, et al., Environ. Sci. Technol. 50 (2016) 4572–4578.
[56] J.Y. Liu, X.Q. Gong, Chin. Chem. Lett. 32 (2021) 1127–1130.
[57] Y.J. Shu, S.M. Liang, J.Y. Xiao, et al., Acta Phys. Chim. Sin. 37 (2021) 2010001.
[58] Z.Y. Fei, S.C. He, L. Li, et al., Chem. Commun. 48 (2012) 853–855.
[59] C.W. Tang, C.C. Kuo, M.C. Kuo, et al., Appl. Catal. A: Gen. 309 (2006) 37–43.
[60] E. Giamello, Z. Sojka, M. Che, A. Zecchina, J. Phys. Chem. 90 (1986) 6084–6091.
[61] Y. Liu, Y. Peng, M. Naschitzki, et al., Angew. Chem. Int. Ed. 60 (2021) 16514–16520.